Sys Rev Pharm 2020;11(12):873-887
A multifaceted review journal in the field of pharmacy

EFFECT OF ATTACKANGLE OF CONCAVE AND CONVEX WINGLET VORTEX GENERATORS ON HEAT TRANSFER AND PRESSURE DROP IN EVAPORATOR FIN AND TUBE HEAT EXCHANGER WITH FIELD SYNERGY PRINCIPLE USING NUMERICAL SIMULATION

SYAIFUL1*; YUNIANTO, Bambang2; SALSABILA, Carisya Dara3; S.U., MSK Tony4, F. SOETANTO, Maria5

1,2,3,4Diponegoro University, Engineering Faculty, Departement of Mechanical Engineering. Indonesia.
5Bandung State Polytechnic, Aerospace Engineering Department, Indonesia

* Correspondingauthor
e-mail: syaiful.undip2011@gmail.com

ABSTRACT

Fin and tube heat exchanger is a type of compact heat exchanger commonly used in refrigeration systems, automotive, aerospace and petrochemical industries. The gas passing through the fin has a lower thermal conductivity than the fluid passing through the tube. The low thermal conductivity results in high thermal resistance, thus the heat transfer rate is low. To enhance heat transfer rate on the fin side, vortex generator is mounted on the fin to generate longitudinal vortex. Longitudinal vortex causes mixing between hot fluid with cold fluid which increases the heat transfer rate. Therefore, this study aims to investigate the effect of the longitudinal vortex generator on the improvement of heat transfer and pressure drop. Numerical simulations were carried out to analyze three types of vortex generators namely Delta Winglet Pairs (DWP), Convex Delta Winglet Pairs (CxDWP), and Concave Delta Winglet Pairs (CDWP) with an inline arrangement and also common flow up configuration (CFU) of winglets. In addition, the installation of VG was varied with the angle of attack between 10o, 15o, and 20o with a 1-3-4-7 VG arrangement on the tube Airflow velocity is expressed in Reynolds number between 364 to 689. Analysis of heat transfer rate enhancement and pressure drop between three types of VG, three variations of attack angle and four types of winglet installation compared to baseline. The simulation results show that the vortex generator with the highest convection heat transfer coefficient is seven pairs of Concave Delta Winglet Pairs (CDWP) at the attack angle of 20o and Re = 689 of 84.85%. While the lowest pressure drop increase of 4.27% was found using one pair of Delta Winglet Pairs (DWP) with the angle of attack of 10o attack and Re = 364.

Keywords:Attack angle; Concave and convex winglet VG; Heat transfer; Pressure drop, Fin and Tube Heat exchanger; Synergy angle

INTRODUCTION

Fin and tube heat exchangers are one of the tools that facilitate heat exchange between two fluids [1]. This compact heat exchanger is widely used in the cooling system, the automotive industry, aerospace, and petrochemical industry. Fin and tube are one of the most widely used compact heat exchangers where gas flows on the fin side. In fact, the gas on the fin side has a high thermal resistance. High thermal resistance causes low convection heat transfer coefficient resulting in low heat transfer. Therefore, improvement of the convection heat transfer coefficient needs to be done by reducing thermal resistance through modification in the fin section [2]. Improved heat transfer by modifying fin (passive method) is an effective method. This fin modification also has an impact on the rise in pressure drop flow which is the concern of many researchers [1].

Gholami et al. (2017) stated that one of the traditional ways to reduce thermal resistance on the gas side is to increase the surface area of the heat exchanger [3]. Fin modification with the protrusion of a surface is used in the heat exchanger to improve overall heat transfer performance. This method is significant to do, especially in the cooling system because high thermal resistance dominates on the gas side. Surface protrusions have various forms such as plain, wavy, louver, slit, offset, and others [4]. However, the surface area protrusions have an impact on increasing the price of production [3]. To overcome this problem, several methods are used to increase the rate of heat transfer. One way to do this is to decrease thermal resistance by thinning the thermal boundary layer between the fluid and the wall [5]. In general, techniques for increasing heat transfer are classified into three main categories, namely active, passive, and combined methods. The active method requires outside energy but is quite complex. Meanwhile, the passive method does not require external energy, but rather by modifying the surface and geometry of a channel. Passive methods are more widely used than active methods because they are economical and easy to produce [6].

Modification with surface protrusion is a passive method that can generate vortices on the fin surface, where this method can increase heat transfer on the gas side [7]. Vortex Generator (VG) is a passive method which is responsible for forming swirling flow and generating vortices. Delta Wings, Rectangular Wings, Delta Winglet

Pairs, and Rectangular Winglet Pairs are types of VGs that can be installed by punching, embossing, welding, or stamping. Two types of vortices caused by VGs are transverse vortices (TVGs) and longitudinal vortices (LVGs) [1]. Transverse vortices are considered less effective than longitudinal vortices. This is because transverse vortices only circulate in the wake VG area, so heat propagation only occurs in that area [8]. Meanwhile, longitudinal vortices trigger secondary flow generation which disrupts the formation of thermal boundary layers and causes flow instability. This flow instability causes turbulence with high scale [9]. In addition, the vortices generated by LVG last a long time until in the downstream region [8].

Various studies on increasing the convection heat transfer coefficient by using a vortex generator have been conducted. Hung-Yi Li et al. (2017) conducted a numerical study to investigate the thermal and fluid characteristics of Pin-Fin Heat Sink using Delta Winglet Vortex Generator [10]. Their results showed that the decrease in thermal resistance in the heat sink is influenced by an increase in Reynolds number and winglet height. A decrease in thermal resistance occurs at an angle of attack of 30 ° with a "common flow up" flow configuration. HermantNaik et al. (2018) carried out three-dimensional modeling to study the effect of winglet locations on heat transfer characteristics in fin and tube heat exchangers using rectangular winglet pairs VG arranged inline [11]. The results show that Nu and Se have maximum values at $\Delta Y = \pm 1.25$ and $\beta = 45$ ° which are mounted in the downstream area adjacent to the tube.

Gaofeng Lu et al. (2018) conducted a numerical study to analyze heat transfer and pressure drop on a fin and oval tube heat exchangers using a tear-drop delta vortex generator [12]. Their results indicated that tear-drop delta VGs have better thermal-hydraulic performance than plain delta VGs. The mechanism of increasing heat transfer was investigated using secondary flow intensity and the field synergy principle. Mohd. Zeeshan et al. (2017) conducted a numerical study to evaluate thermal-hydraulic performance on fin and tube heat exchangers using oval and flat tube types in inline and staggered installations [13]. The overall simulation results stated that the oval tube has the highest ratio by analyzing performance evaluation criteria (PECs). The increase in heat transfer coefficient occurred by 13.99% on the gas side with a low Reynolds number (Re = 400) and 4.99% with a high Reynolds number (Re = 900). Nares Chimres et al. (2018) conducted a numerical study to optimize the design of semi-dimple vortex generators on fin and tube heat exchangers [14]. The results showed that the greatest goodness factor is obtained at an angle of attack of 30º, VD = 5.5 mm, and HD = 7.5 mm in each semi-dimple diameter. This type of VG experiences an increase in goodness factor of 33-37% after being redesigned and increases 15-20% better than plain fin.

Salleh et al. (2019) investigated experimentally and numerically the thermal-hydraulic performance of fluid flow that passes through the fin and tube heat exchanger with and without using a trapezoidal winglet vortex generator (TWVG) [15]. The experimental results showed that heat transfer could be increased by variations in geometry, installation configuration, aspect ratio (Λ), and specific angle of attack (β) on TWVG. Meanwhile, numerical simulation results illustrated that flat trapezoidal winglets mounted with a common flow-up orientation at $\Lambda = 3$ and $\beta = 10$ ° have the best thermal-hydraulic performance. This performance is found based on increased heat transfer and decreased pressure drop. Gaofeng Lu et al. (2019) conducted numerical simulations to evaluate heat transfer performance and flow structure using curved vortex generators on fin and tube heat exchangers [16]. Their results showed that the intensity of the secondary flow was higher with the greater radius of curvature in the curved VG. Vortex generators with curvature of 0.25, $\beta = 15$ °, and R = 1.06 have the best thermal-hydraulic performance.

Syaiful et al. (2017) studied experimentally to analyze the effect of concave rectangular winglet pairs VG on thermal-hydraulic performance on flow in channels [17]. The experimental results showed an increase in convection heat transfer coefficient using CRWP VG by installing three pairs and 45° attack angle by 188% compared to the baseline. However, the addition of VG pairs and attack angles results in an increase in pressure drop. KeWei Song et al. (2019) conducted a numerical study to determine the characteristics of heat transfer with the use of concave and convex curved vortex generators in channels in the laminar flow [18]. Their results showed that concave curved VG could improve heat transfer better than curved convex VG and plain VG. Concave curved VG has a higher JF value at Re = 1400, $\beta = 20$ °, and $\theta = 80$ °, which is 11.3% compared to that of convex curved VG. Yonggang Lei et al. (2017) conducted a numerical study to improve thermal-hydraulic performance in a circular tube using punched delta winglet vortex generators [19]. Their results showed that the increase in Nusselt numbers was influenced by the reduction in pitch diameter in the delta winglet VG. The mechanism of increasing heat transfer affected by VG was examined using the field synergy principle.

Zhimin Han et al. (2018) conducted a numerical study to determine the heat transfer characteristics of a rectangular winglet vortex generator that was added by a hole [20]. Their results showed that VG with holes has better thermal-hydraulic performance than without holes. In addition, the optimal VG hole diameter is at d = 5 mm through analysis of PEC values, Colburn factor, and friction factor. Mohammad Oneissi et al. (2018) conducted numerical simulations to compare the increase in heat transfer between delta winglet pairs (DWP) and inclined delta winglet pairs (IDWP) with hemispherical protrusions in the downstream area [21]. Their results showed that the IPWP-M configuration could increase heat transfer, respectively 7.1% and 2.3% better than that of the DWP and IPWP. Meanwhile, an increase in heat transfer of 3.2% was found in the use of DWP-PRO1.

Syaiful et al. (2018) investigated numerically to increase heat transfer in fin and tube heat exchangers through the addition of pairs to the concave rectangular winglet vortex generator [22]. Numerical simulation results showed that the highest increase in convection heat transfer coefficient is found in seven rows of RWP and CRWP, respectively for 38.1% and 102.5% with an attack angle of 15º. The longitudinal vortex produced by CRWP is stronger than RWP so that CRWP can increase the higher convection heat transfer coefficient. Based on previous research, an increase in convection heat transfer coefficient was always accompanied by an increase in pressure drop, which causes low thermal-hydraulic performance. In this study, numerical simulations are based on experiments on evaporators conducted by Joardar and Jacobi (2008) [23]. Two new types of VG, concave delta winglet pairs (CDWP) and convex delta winglet pairs (CxDWP), is compared to delta winglet pairs (DWP) and baseline with variations in attack angles (α), 10 °, 15 °, and 20 °, in which study using CDWP and CxDWP is still rarely conducted in previous studies. Therefore, this study is aimed at improving convection heat transfer and pressure drop with variations in VG types and attack angles at fin and tube heat exchanger.

MODEL DESCRIPTION:

PHYSICAL MODEL

3D numerical simulation was performed on three types of VG by varying three kinds of attack angles and four types of VG installations arranged in a "common flow up". Figure 1 shows the isometric type of VG used. Meanwhile, detailed VG geometry is shown in Figure 2.

The distance between the trailing edge of the three types of vortex generator and the midpoint of the tube is 6.4 mm. For concave and convex VG, the radius of curvature was set at 21 mm. VG has a height (H) of 60% of the channel height, as can be seen in Figure 3. The angle of attack (α) was varied at 10 °, 15 °, and 20 °. The installation configuration was performed on the vortex generator for successive tubes, namely one VG pair on the first tube; three pairs of VG in the first, third and fifth tubes; four VG pairs in the first, third, fifth and seventh tube; and seven VG pairs are in the entire tube.

Determination of the computational domain in the numerical model can be seen in Figure 4, where the Cartesian coordinates (x, z) express the direction of streamwise and spanwise flow, and coordinates (z) are normal flow towards the wall. Dashed lines are computational domains that are used as modeling geometries. The fin mounted on the top and bottom form a channel that has a height of H = 3.63, length L = 177.8 mm, and width B = 12.7 mm. Fin material used aluminum with a fin thickness of Ft = 0.18 mm. The distance between the inlet and the midpoint of the first tube is 12.7 mm, while the distance between the next tube and the outer diameter of the tubes (P1 and Ps) are 25.4 mm and D = 10.67 mm, respectively. In fin and tube heat exchangers, heat transfer is dominated by convection. However, conduction heat transfer at fin is expressed in the form of temperature distribution and cannot be ignored entirely [24], so the calculation of conjugate heat transfers was carried out in this modeling. Therefore, the side-view computational domain in Figure 4 (b) expressed by the dotted line was chosen to solve the conjugate heat transfer case.

Figure 5 is a computational domain in 3-D form. The computational domain has three parts consisting of the extended upstream region, extended downstream region, and fin coil region. The extended upstream region is the extension region of the inlet to ensure that the flow entering the channel is fully developed. The fin coil region is located between the upstream and downstream areas, where there are a vortex generator and tube installation. In addition, the addition of extended outlets (extended downstream region) was carried out so that no reverse circulation occurs when the fluid flow is out.

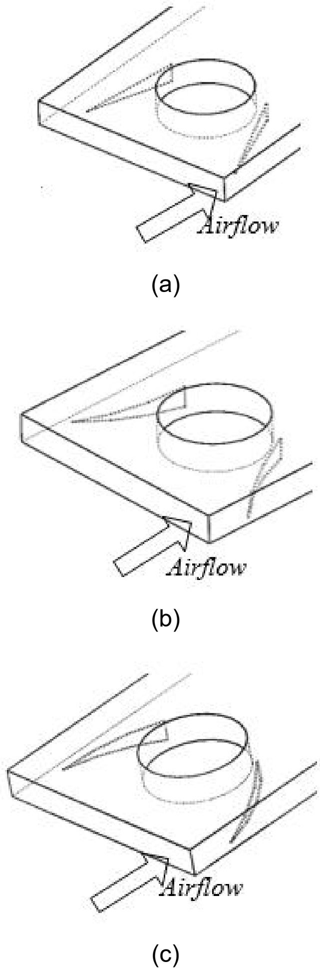

Figure 1. Geometry of vortex generator; (a) Delta winglet pairs; (b) Convex delta winglet pairs; (c) Concave delta winglet pairs.

GOVERNING EQUATIONS

In this 3D numerical simulation, the gas passing through the fin was assumed to be an incompressible flow with constant physical properties. The Reynolds number was in the range of 364 - 689, so the flow was assumed to be laminar. The thickness of the fin and conduction heat transfer at the fin are the parameters to determine the temperature distribution at the fin surface. Based on these assumptions, the governing equation used to solve this case is

Continuity equation

$$\frac{\partial}{\partial x_i}(\rho u_i) = 0 \quad \text{(Eq. 1)}$$

Momentum equation

$$\frac{\partial}{\partial x_i}(\rho u_i u_k) = -\frac{\partial p}{\partial x_k} + \frac{\partial}{\partial x_i}\left(\mu \frac{\partial u_k}{\partial x_i}\right) \quad \text{(Eq. 2)}$$

Energy equation

$$\frac{\partial}{\partial x_i}(\rho u_i T) = \frac{\partial}{\partial x_i}\left(\Gamma \frac{\partial T}{\partial x_i}\right) \quad \text{(Eq. 3)}$$

where ρ, p, u, μ, and T are density, pressure, average velocity on the x-axis, the dynamic viscosity of air, and temperature, respectively. Γ is the diffusion coefficient which is defined as $\Gamma = \frac{\lambda}{c_p}$, where λ and $c_p$are fluid and specific thermal conductivity respectively.

2.3. Boundary conditions

The boundary conditions for all computational domains are described as follows:

1. Upstream extended region
   - At the inlet boundary

$u = u_{in}, v = w = 0, T = T_{in} = cons.$ (Eq. 4)

   - At the top and bottom boundaries

Velocitycondition: *periodiccondition*$u_{up} = u_{down}$

Temperaturecondition: *periodiccondition*$T_{up} = T_{down}$

2. Downstream extended region
   - At the outlet boundary

$$\frac{\partial u}{\partial x} = \frac{\partial v}{\partial x} = \frac{\partial w}{\partial x} = \frac{\partial T}{\partial x} = 0 \quad \text{(Eq. 5)}$$

   - At the top and bottomboundaries

Velocitycondition: *periodiccondition*$u_{up} = u_{down}$

Temperaturecondition: *periodiccondition*$T_{up} = T_{down}$

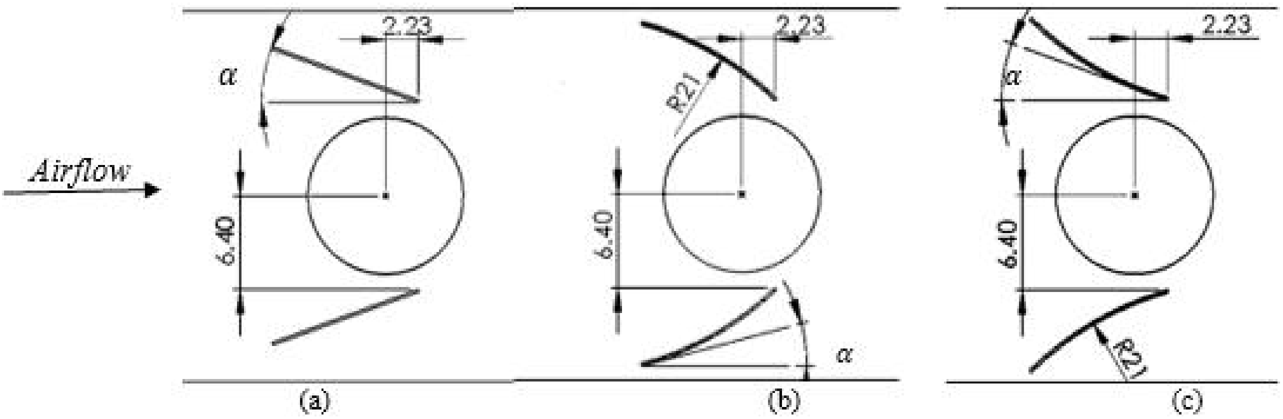

Figure 2.The dimensions of the vortex generator and their placement on the tube; (a) Delta winglet pairs; (b) Convex delta winglet pairs; (c) Concave delta winglet pairs

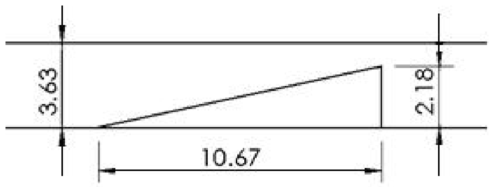

Gambar3. Vortex generator dimension (side view)

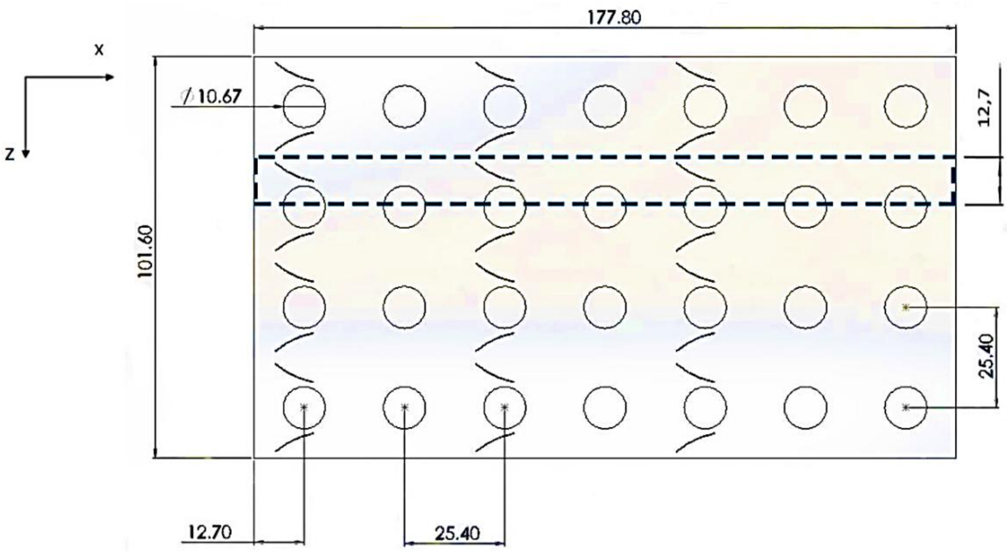

(a)

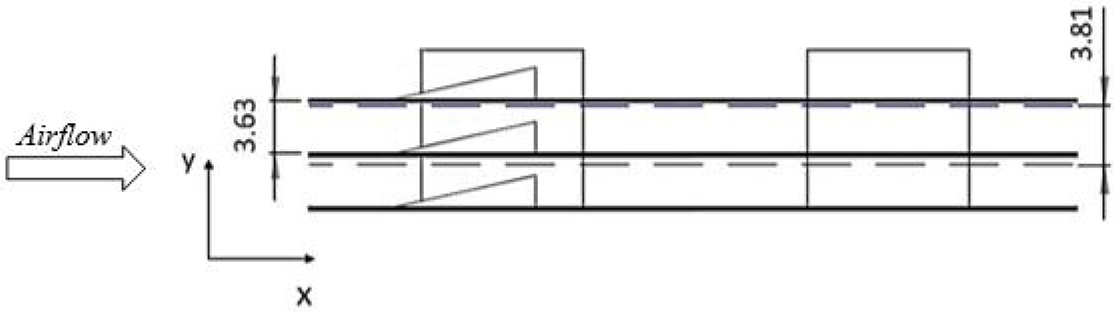

(b)

Figure 4. Computational domain in fin and tube heat exchanger; (a) top view, (b) side view

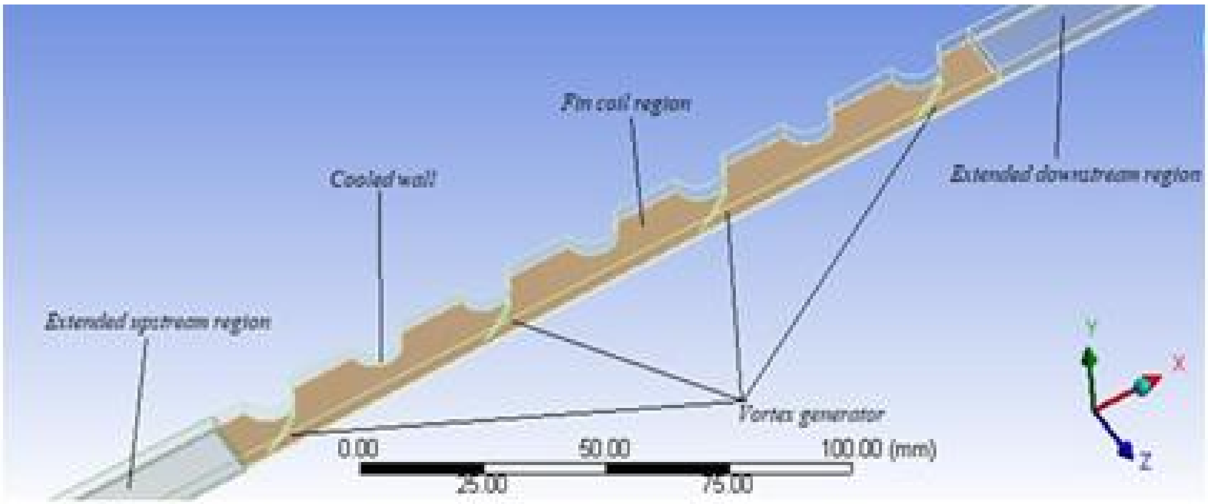

Figure 5. Computational domain

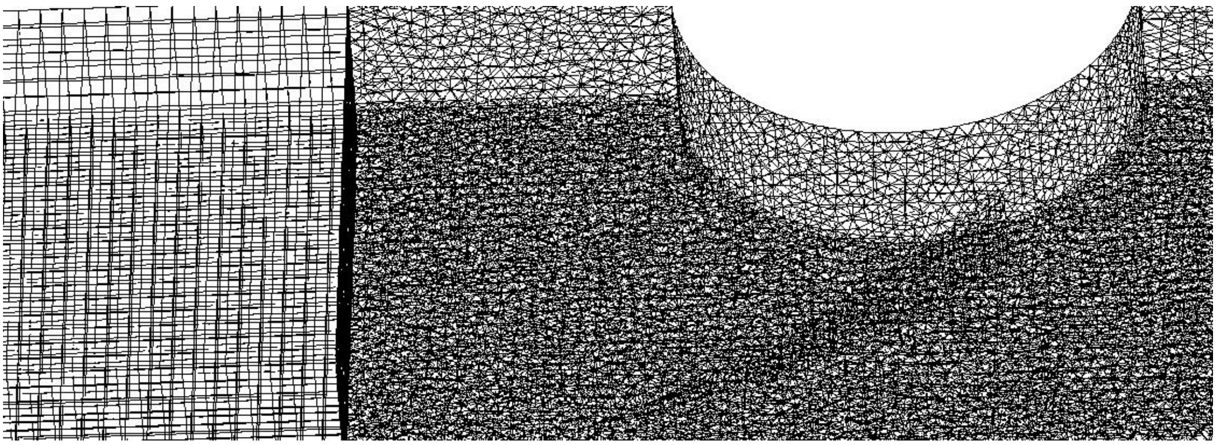

Figure 6.Meshing

3. Fin coil region
   - At the top and bottomboundaries

Velocitycondition: *periodiccondition* $u_{up} = u_{down}$

Temperaturecondition: *periodiccondition* $T_{up} = T_{down}$

- At the side boundaries

Cooled wall $u=v=w=0, T=T_w$ (Eq. 6)

4. Symmetry

$$V = 0, \frac{\partial u}{\partial y} = \frac{\partial w}{\partial y} = \frac{\partial T}{\partial y} = 0 \quad \text{(Eq. 7)}$$

NUMERICAL METHOD

The geometry used in 3-D simulations has a complex shape so that high accuracy is required to obtain good results. The accuracy of the shape and size of the geometry can be determined by adjusting the shape and type of the mesh.The computational domain mesh is shown in Figure 6. The type of mesh used for the extended upstream region and the extended downstream region is hexahedral.This type of hexahedral mesh is used because the extended upstream region and the downstream region have simple shapes. Meanwhile, the VG and tube domain has complex geometry so that tetrahedral mesh was applied in this domain for higher accuracy.

The governing equations of (1) - (3) by determining boundary conditions (4) - (7) were solved by using Computational Fluid Dynamics (CFD).Thelaminer model was used in the current simulation. The SIMPLE algorithm was used to solve the correlation between velocity and pressure. The governing equation for momentum and energy was discretized with the second order upwind scheme.The convergence criteria in this simulation were set 10^{-5} for continuity equations and 10^{-8} for energy equations.

Parameters definition

The parameters used in this study are as follows:

Reynolds number

$$Re = \frac{\rho\, u_m\, D_h}{\mu} \quad \text{(Eq. 8)}$$

Nusselt number

$$\overline{Nu} = \frac{h\, D_h}{\lambda} \quad \text{(Eq. 9)}$$

where ρ, u_m, μ, and, λ are the density, average velocity of the fluid in the direction of flow, dynamic viscosity, and thermal conductivity. D_h is the hydraulic diameter which is formulated as $D_h = 4(A_{min}L)/A_T)$. The convection heat transfer coefficient (h) is defined as:

$$h = \frac{q}{A_T \Delta T} \quad \text{(Eq. 10)}$$

where q, AT, and ΔT are the convection heat transfer rate, the total surface area of the heat transfer, and the average logarithmic temperature difference.

The total heat transfer and the difference in average logarithmic temperature are described in the following equation:

$$q = \dot{m}c_p(\overline{T}out - \overline{T}in) \quad \text{(Eq. 11)}$$

$$\Delta T = \frac{(T_w - T_{in}) - (T_w - T_{out})}{\ln\left[(T_w - T_{in})/(T_w - T_{out})\right]} \quad \text{(Eq. 12)}$$

where T_w, T_{in}, and T_{out} are cooled wall temperature, inlet temperature, and outlet temperature, respectively. Whereas, $\dot{m}$ is the mass flow rate, $\dot{m} = \rho u A_c$, where A_c is the cross-sectional area when fluid flow enters the channel.

London goodness factor is defined as the ratio of colburn factor (j) and friction factor (f) expressed in the following equation:

$$j = St.Pr^{2/3} \quad \text{(Eq. 13)}$$

$$St = \frac{h}{\rho U_m c_p} \quad \text{(Eq. 14)}$$

$$f = \frac{2\,\Delta P}{\rho\, U_m^2 \frac{A_T}{A_{min}}} \quad \text{(Eq. 15)}$$

where A_{min} is the minimum cross-sectional area. ΔP is the pressure drop of fluid flow through the heat exchanger which is formulated as $\Delta P = P_{in} - P_{out}$.

VERIFICATION

An independent grid test is carried out to ensure that the simulation results do not depend on the number of grids. Independent grid tests were carried out at Reynolds number of 524. Three grid numbers (1,200,000, 1,400,000 and 1,600,000) were tested in which 1,400,000 grids were selected as independent grids. This independent grid was chosen because the value of the heat transfer coefficient obtained almost did not change after the number of grids was added.

In this work, geometry was made according to experiments carried out by Joardar and Jacobi [23]. Validation was performed by comparing the value of convection heat transfer coefficient and pressure drop from the simulation and experimental results in the range of Reynolds numbers 523 to 942, as reported in Figure 7.

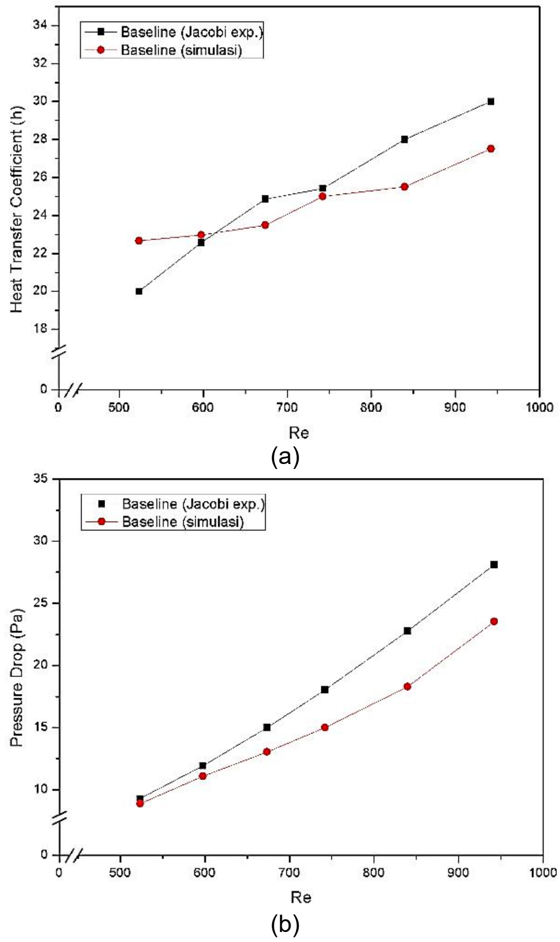

Figure 7. Comparison Joardar and Jacobi's experiment and present study for (a) Heat transfer coefisien, and (b) pressure drop

RESULTS AND DISCUSSION:

This study aims to determine the effect of variations in VG shape, angle of attack, and number of VG installations on flow structure and thermal-hydraulic performance.Vortex generators are an efficient method for increasing convection heat transfer by enhancing flow turbulence and disrupting the formation of thermal boundary layers [16].

VELOCITY STREAMLINE AND VECTOR

Figure 8 shows the streamline at Re = 689 by comparing installations without VG (baseline), and installation of seven pairs of VGs. From Figure 8, it was found that different flow patterns are ob-

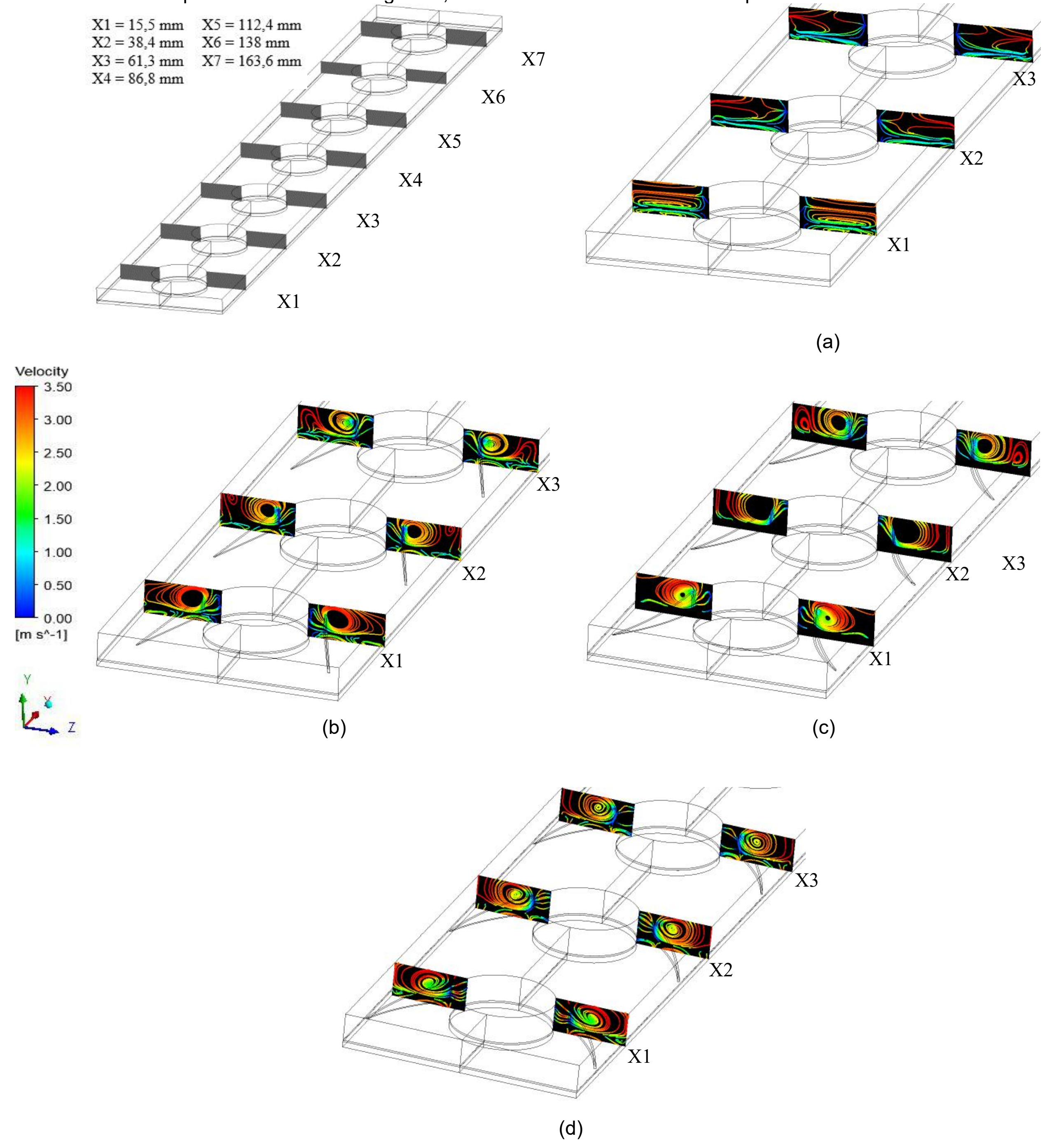

Figure 8. Comparison of streamline of longitudinal vortex at several cross-sections area for Re = 689 dan α = 20º for: (a) baseline; (b) seven pairs of DWP VGs; (c) seven pairs of CxDWP VGs; and (d) seven pairs of CDWP VGs

served for the use of different vortex generators. The streamline at the baseline shows a uniform flow velocity distribution, as in Figure 8 (a), while the use of VG generates swirling motion in the flow. Swirling motion in the wake area of the VG indicates the formation of longitudinal vortices which facilitate fluid exchange in the main flow and the area near the wall [25]. With a common flow-up flow orientation, the generation of longitudinal vortices has a counter-rotating direction that is formed due to the interaction of centrifugal forces, and the difference in pressure in the spanwise direction [26]. Counter-rotating longitudinal vortices produce downwash regions that carry the flow from the main flow towards the wall and upwash regions that carry outflow into the main flow [27]. Swirl flow is clearly observed with the influence of VG geometry, as shown in Figure 8 (b) - (d). CDWP geometry produces a stronger swirl flow than that of CxDWP because the frontal surface of CDWP is wider than CxDWP. However, swirl flow (longitudinal vortices) generated by a pair of VGs is observed to weaken in the downstream direction. Longitudinal vortices that are formed cannot last long because of the recirculation effect of the flow behind the tube [11]. Therefore, the addition of VG pairs is performed to overcome this problem. Longitudinal vortices fade after passing through the first wake region and are reinforced with VG in the second row when the flow hits the leading edge of the winglet. Installation of VGs in each tube enhances counter-rotating longitudinal vortices so that swirl flow can last until downstream.In addition, the orientation of the common flow-up causes the vortices on the left to rotate clockwise and on the right to rotate counter-clockwise in the direction towards the center of the channel. Both of these vortices destroy the thermal boundary layer resulting in a high increase in heat transfer [28]. As observed in Figure 9, the main vortex and corner vortex are produced in the downstream of VGs. Separation at the leading edge of the winglet results in the main vortex, while the corner vortex originates from the junction between the fin and the stagnation area caused by the difference in pressure on the winglet side (see Figure 9) [25].

Comparison of tangential velocity vectors in cross-section area with common flow-up orientation in DWP, CxDWP, and CDWP is shown in Figures 10. Vorticities are clearly observed behind VGs through the cross-section plane (spanwise). The intensity of the longitudinal vortex fades into the downstream region due to viscous dissipation [25], and it will be strengthened by the VGs behind it. Based on streamline and tangential velocity vectors, CDWP produces the greatest vortices with strongest intensity than those from CxDWP and DWP

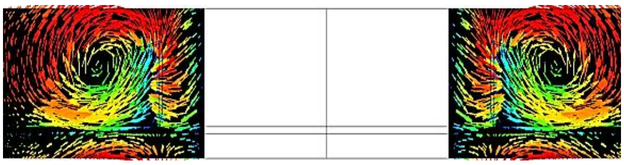

Figure 9. Main vortex and corner vortex at installation of seven pairs of CDWP with Re = 689 and α = 20° at x/L = 15.5

3.2. Longitudinal vortex intensity

Longitudinal vortex intensity is the ratio of inertia force induced by secondary flow to viscous force as stated by KeWei Song, et al. [2]. Longitudinal vortex intensity (Se) is obtained through Equation (17).

$$Se = \frac{\rho D_h U}{\mu} \qquad \text{(Eq. 17)}$$

whereas U represents the secondary flow velocity characteristics expressed in Equation (18).

$$U = D_h|\omega^n| = D_h\left|\frac{\partial w}{\partial y} - \frac{\partial v}{\partial z}\right| \qquad \text{(Eq. 18)}$$

where ω^n represents the vorticity component in the normal direction with respect to the transverse axis. The mean longitudinal vortex intensity in the spanwise direction is defined as:

$$Se_x = \frac{\rho D_h^2}{A(x)\mu}\iint_{A(x)} |\omega^n| dA \qquad \text{(Eq. 19)}$$

Figure 11 shows a comparison of the local longitudinal vortex intensity (Se_x) for seven pairs of VGs at different attack angles. From Figures 11, it is observed that the longitudinal vortex intensity produced by the CDWP is stronger than that of the DWP due to the instability of the centrifugal force when the flow passes through the concave wall [29]. For the CxDWP case, the convex geometry narrows the channel so that the flow through the VG and tube is accelerated, and the longitudinal

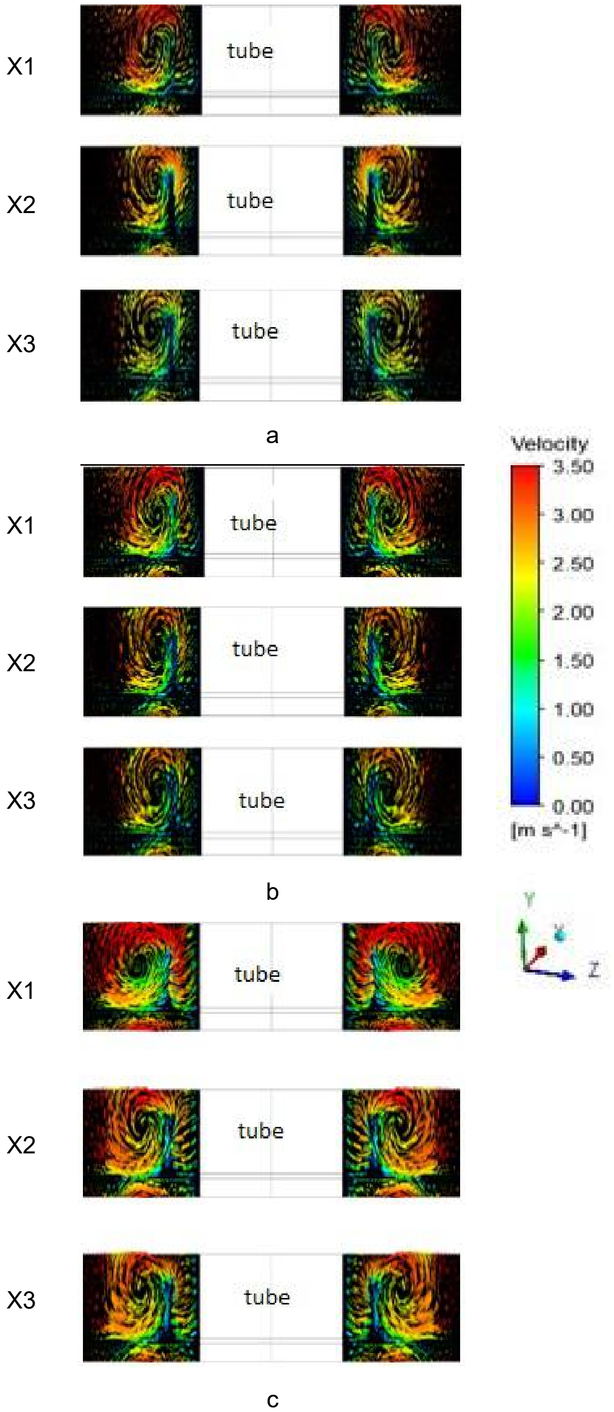

Figure 10. Tangential velocity vector of seven pairs VGs at location X1, X2, and X3 for Re = 689 at angle attack of 20° in the case of; a. DWP; b. CxDWP, and c. CDWP

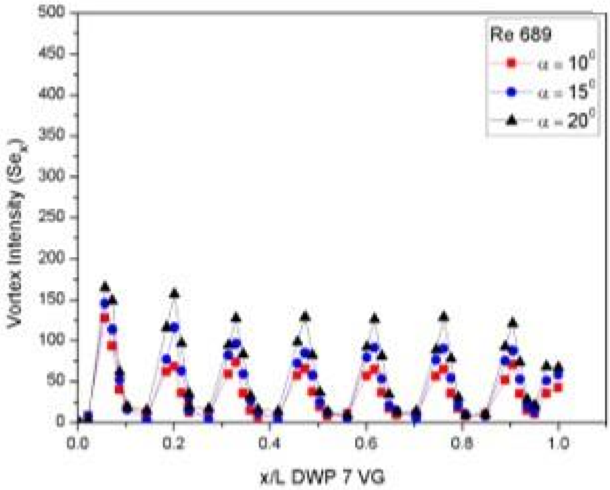

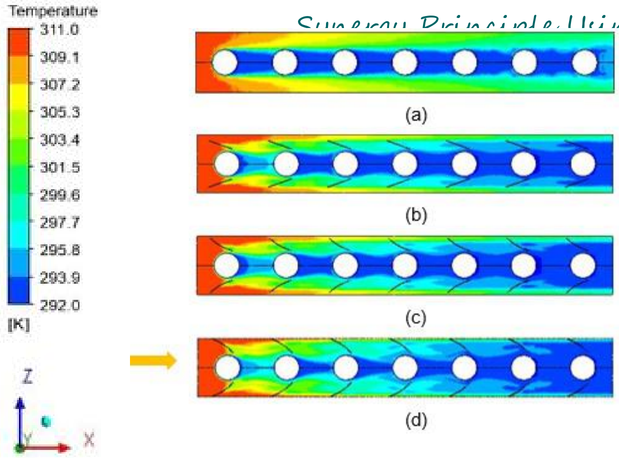

Figure 12. Temperature distribution for seven pairs of VGs in streamwise section at Re = 689 and attack angle of 20° for the case of: a. baseline, b. DWP, c. CxDWP, and d. CDWP

vortex that is generated is stronger than that of the DWP. However, the pressure difference on the downstream and upstream side of CxDWP is lower than that of the CDWP so that the longitudinal vortex produced is weaker [18]. An increase in the angle of attack from 10º to 20º enhances the intensity of the longitudinal vortex, which means stronger vortex circulation [17]. From Figure 11, it is observed that the decrease in the longitudinal vortex on a single VG pair is caused by viscous dissipation when the flow is going downstream. However, the longitudinal vortex is enhanced again with the addition of VG pairs [12]. In Figures 11 (a) - (c), it was found that the increase in the longitudinal vortex intensity for the installation of seven pairs of CxDWP and CDWP is 36.9% and 185.23%, respectively, against DWP at Re = 689 with an attack angle of 20º at x/L = 0.21.

TEMPERATURE DISTRIBUTIONS

Figure 12 illustrates the temperature distribution for baseline, DWP, CxDWP, and CDWP cases in an installation configuration of seven pairs of VGs with Re = 689 and an attack angle of 20°. The temperature distribution is observed in the streamwise direction at Y = 1.5 mm. From Figure 12, it is found that low temperature is seen behind the tube, and high temperature is observed in front of and on the side of the tube due to horseshoes and longitudinal vortices [11]. Low temperatures are distributed in the wake region where the flow velocity is relatively slow, and heat transfer is low In order to increase heat transfer, the wake region is weakened so that the fluid mixture increases. VG installation induces a high-temperature gradient around VG, and secondary flow is generated. Then, secondary flow mixes with the flow in the area of the tube wake, which causes thinning of the thermal boundary layer and a significant increase in heat transfer [30]. By paying attention to Figure 18, it is observed that CDWP has the best temperature distribution than that of CxDWP and DWP. CDWP generates the strongest longitudinal vortex because of the influence of the centrifugal force on the surface curvature of the VGs. Vortices carry cold fluid from the tube wake to the main flow and vice versa. This narrows the area of the tube wake and results in a high-temperature gradient [1].

The generation of longitudinal vortices by VG causes thinning of the thermal boundary layer in the downwash region of the wake tube, where an increase in heat transfer occurs. After passing through the downwash region, the boundary layer again thickens in the upwash region. The addition of VG pairs reinforces the longitudinal vortex so that the fluid is mixed evenly with the installation of VG to the downstream region.

From Figure 13 (a), a low temperature was observed in the area near the wall at x/L = 0.084 and Re = 689 for the baseline case. For the same case, the installation of VG causes the high temperature distributed in the main flow to be mixed with low temperatures in the area near the wall, as described in Figure 13 (b) - (g). This is caused by the generation of longitudinal vortices, which increases mixing and results in thinning of the thermal boundary layer [19]. From Figures 13 (b) - (g), it is found that the temperature gradient is more evenly distributed with an increasing angle of attack which indicates a stronger mixing of the fluid in the main flow and near the tube wall [5].

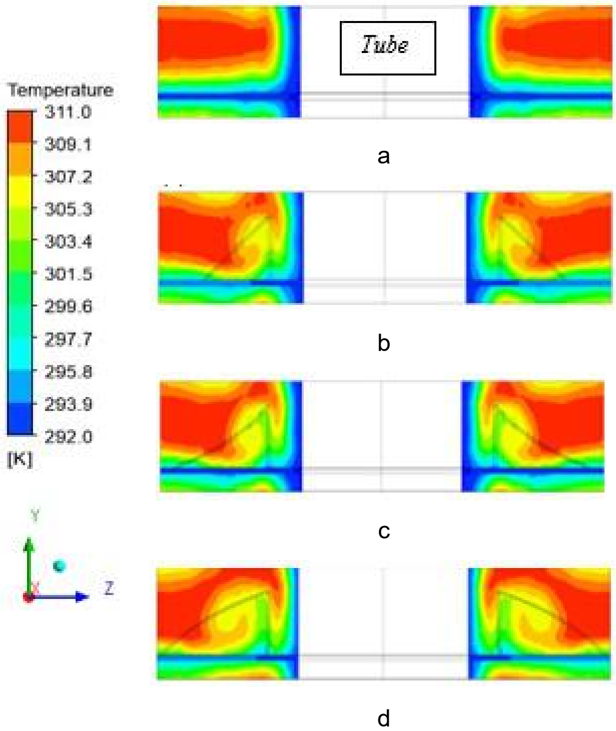

Figure 13. Temperature distribution with seven pairs of VGs at Re = 689 and attack angle 20° for x/L = 0.084 behind first pair of VGs for the case of: a. baseline, b. DWP, c. CxDWP, and d. CDWP

effect of the Reynolds number on the convection heat transfer coefficient (h) for the DWP, CxDWP, and CDWP cases is shown in Figure 15. The convection heat transfer coefficient increases with increasing Reynolds number. This is because the generation of longitudinal

PRESSURE DISTRIBUTIONS

Figure 14 illustrates the comparison of pressure distribution at baseline and for the case of seven pairs of DWP, CxDWP, and CDWP with Re = 689 and an attack angle of 20º. It can be observed that CDWP has the highest pressure drop. This is because concave geometry has a broader frontal area that inhibits the main flow rate [14]. Whereas the increase in pressure drop for the CxDWP case is lower than that of CDWP. The longitudinal vortex generated by CxDWP is lower than that of CDWP, so the flow resistance is smaller [18].

EFFECT OF ANGLE ATTACK ON THE CONVECTION HEAT TRANSFER COEFFICIENT (H)

The increase in convection heat transfer coefficient is influenced by an increase in Reynolds number, the geometry of VG, the angle of attack to the fin and tube heat exchanger. The

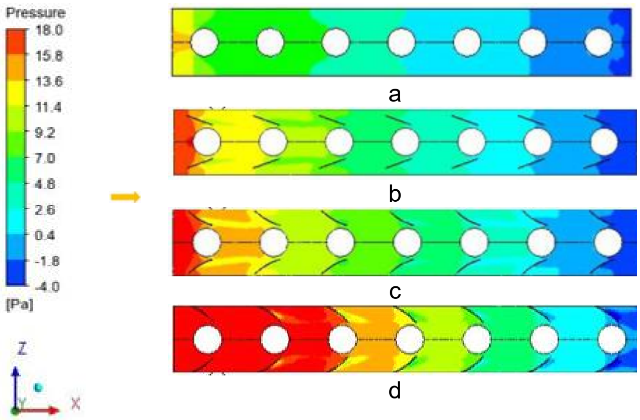

Figure 14. Pressure distribution at Re = 689 and α = 20° for; (a) *baseline* (b) seven pairs of DWP VGs; (b) seven pairs of CxDWP VGs; and (c) seven pairs of CDWP VGs

vortices by high-velocity flow is stronger than low-velocity flow [9]. In addition, CDWP produces higher convection heat transfer coefficients than those of CxDWP and DWP because of the wider contact area [17]. The flow that passes through the concave area experiences instability caused by the centrifugal force on the curvature of the CDWP. This flow instability generates a strong longitudinal vortex [29]. Increasing the angle of attack can increase the convection heat transfer coefficient. Longitudinal vortex strength increases with an increasing angle of attack. This results in the exchange of cold fluid near the wall with the hot fluid in the main flow and the generation of secondary flow have an impact on increasing the convection heat transfer coefficient [25]. Enhancement of heat transfer occurs when the flow through the first pair of VG triggers the generation of longitudinal vortices and fades in the wake area. Furthermore, the addition of VG pairs revives the longitudinal vortex with a higher intensity and increases the convection heat transfer coefficient [2]. At an angle of attack of 10° and Re = 689, the increase in convection heat transfer coefficients for DWP, CxDWP, and CDWP cases is 33.76%, 43.59%, and 73.01%, respectively, against the baseline. Meanwhile, the increase in convection heat transfer coefficient to baseline at DWP, CxDWP, and CDWP is 41.11%, 49.42%, and 79.50%, respectively, with an attack angle of 15° and Re = 689. An increase in maximum convection heat transfer coefficient is found at the attack angle of 20º and Re = 689 for DWP, CxDWP, and CDWP cases of 50.25%, 57.71%, and 84.85%, respectively to the baseline. However, an increase in the convection heat transfer coefficient with an increase in the Reynolds number, the geometry of the VG,

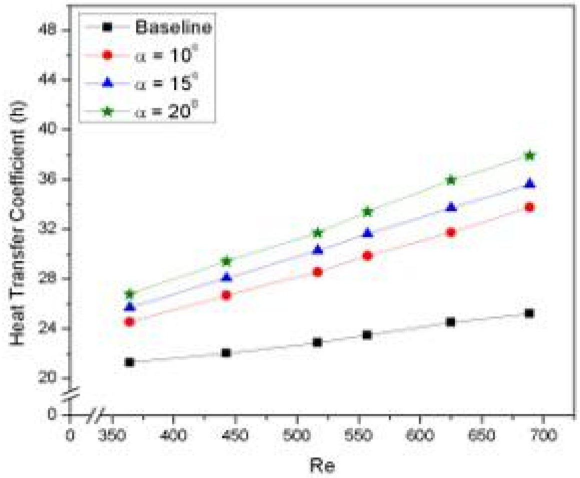

A

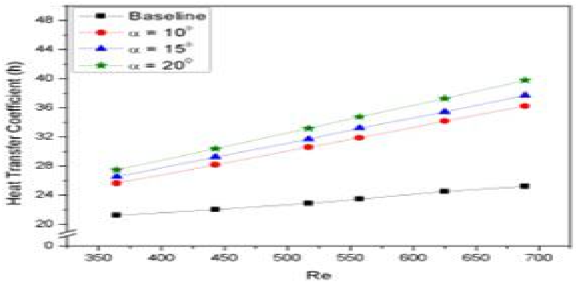

b

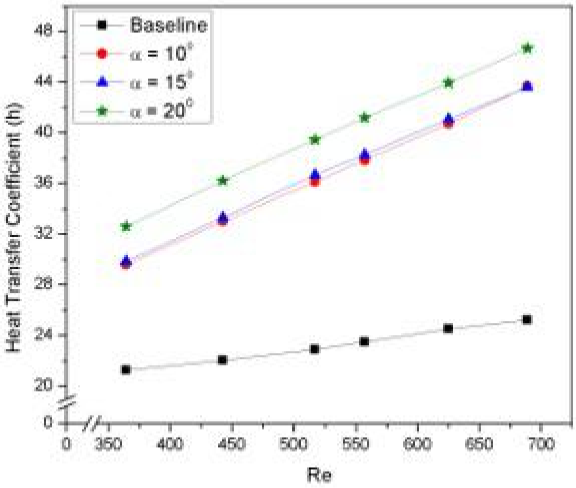

c

Figure 15. Comparison of convection heat transfer coefficient with variation of attack angles at seven pairs of VG for case: (a) DWP ; (b) CxDWP; dan (c) CDWP

the angle of attack, and the addition of pairs have an effect on increasing the pressure drop [26].

Effect of parameters on pressure drop (∆P)

In addition to an increase in the convection heat transfer coefficient, VG installation causes an increase in pressure drop due to obstruction of the main flow on the airside [31]. Pressure drop increases with increasing Reynolds number. The flow that passes through the VG with a common flow up orientation reinforces the frictional forces on the wall and the local resistance of the VG, which results in an increase in pressure drop [28]. Figure 16 shows the comparison of pressure drop for CDWP, CxDWP, and DWP cases with variations of attack angles, and Reynolds numbers from 364 to 689. As in the previous cases, the drag force generated from CDWP is higher than that of CxDWP and DWP. This results in the extent of the recirculation region behind the VG, which enlarges the drag force [15]. The installation of seven pairs of VG results in the increase in heat transfer coefficient. However, these results in an increase in pressure drop, as observed in Figure 16. The increase in pressure drop for the seven pairs of DWP, CxDWP, and CDWP cases is 49.07%, 58.24%, and 128.74%, respectively, against the baseline at the attack angle of 10º to 20º. The increase in the intensity of the longitudinal vortex in CDWP cases due to differences in pressure and friction is higher than that of CxDWP and DWP [32]. This causes the highest increase in pressure drop on the use of CDWP VG.

3.7. Effect parameter on thermal-hydraulic performance

From the study, an increase in convection heat transfer rate is followed by an increase in pressure drop. London goodness factor (j/f) is used to evaluate the overall thermal-hydraulic performance of fin and tube heat exchangers [28]. London goodness factor is the ratio between the Coulburn j factor and friction factor, which is represented by convection heat transfer coefficient and pressure drop, respectively. Figure 17 shows a comparison of the London goodness factor for DWP, CxDWP, and CDWP cases by varying the angle of attack for the seven pairs of VGs. The increase in the angle of attack causes a decrease in thermal-hydraulic performance due to an increase in pressure drop caused by the drag force of VG. As observed in Figure 17, the decrease in the j/f ratio is clearly observed in the installation of seven pairs of VGs. At an angle of attack of 10°, the ratio j/f for seven pairs of DWP, CxDWP, and CDWP is found to be 0.231, 0.229, and 0.206, respectively, against the baseline. Meanwhile, the j/f ratio of the seven pairs of DWP, CxDWP, and CDWP to the baseline with an attack angle of 15° is 0.229, 0.225, and 0.195, respectively. j/f ratio for the case of seven pairs of DWP, CxDWP, and CDWP to the baseline is observed 0.225, 0.221, and 0.178, respectively, with an attack angle of 20°.

3.8. Field synergy principle analysis (FSP)

Field Synergy Principle (FSP) is a method to find out the increase in heat transfer developed by Guo et al.[33]. Increased heat transfer is expressed by decreasing the intersection angle between the velocity vector and the temperature gradient which is defined as the synergy angle. Based on the study of Guo et al. [33], synergy angle is obtained through the energy balance equation as revealed in Equation (20) through Equation (23):

$$\rho C_p \int_0^{\delta_t} (U.\nabla T)\, dy = -\lambda \frac{\partial T}{\partial y} \qquad \text{(Eq. 20)}$$

whereρ, c_p, dan λ is assumed to be constant, so the dimensionless form of Equation (20) is

$$Re_x Pr \int_0^1 \left(\bar{U}\nabla\bar{T}\right) d\bar{y} = Nu_x \qquad \text{(Eq. 21)}$$

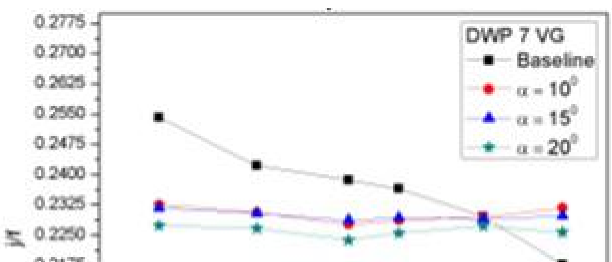

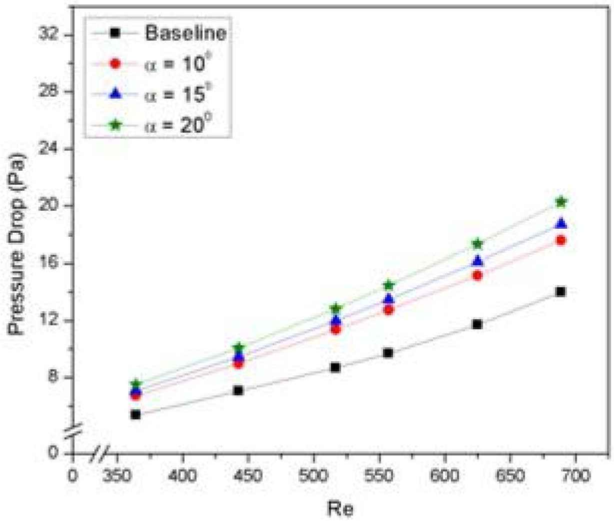

a

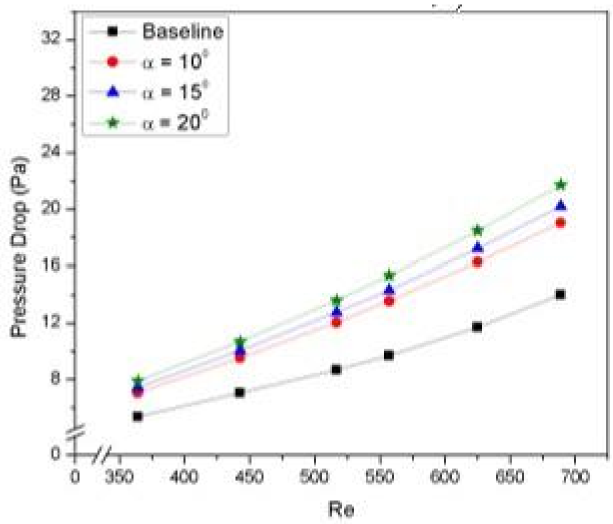

b

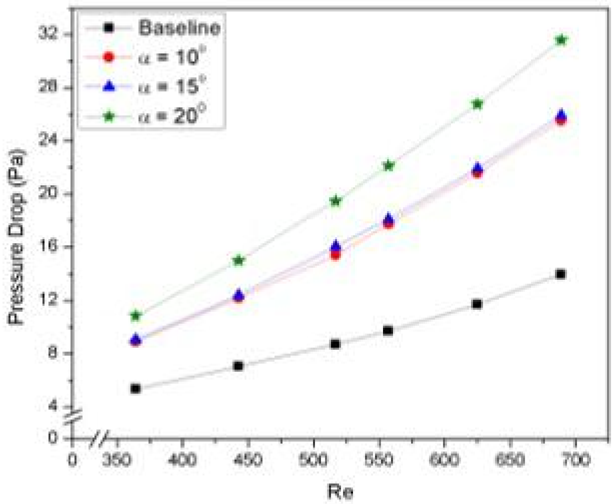

c

Figure 16. Comparison of pressure drop with variation of attack angles at seven pairs of VGs for thecase: (a) DWP ; (b) CxDWP; dan (c) CDWP

where $\bar{U} = \frac{U}{U_\infty}$, $\nabla\bar{T} = \frac{\nabla T}{(T_\infty - T_w)/\delta_t}$, $\bar{y} = \frac{y}{\delta_t}$. $U_\infty$and $T_\infty$are the velocity and temperature of the fluid, respectively, in the

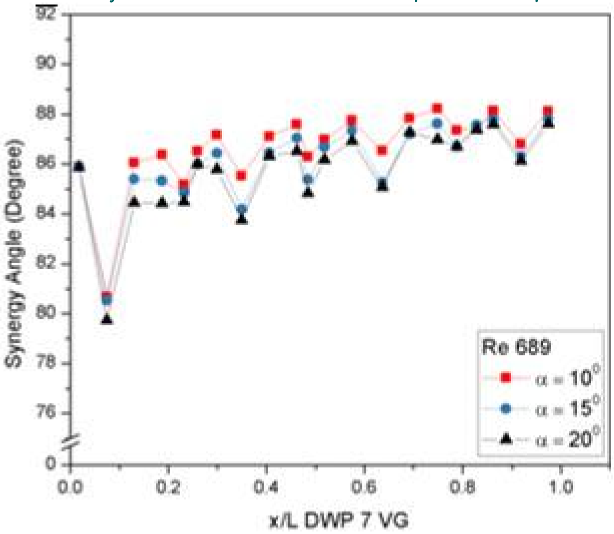

a

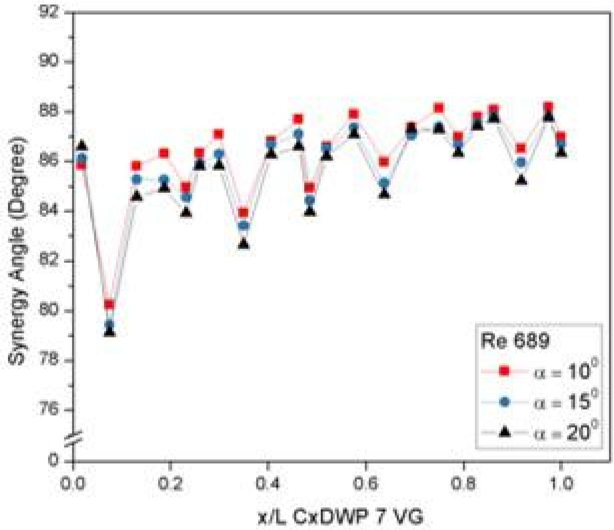

b

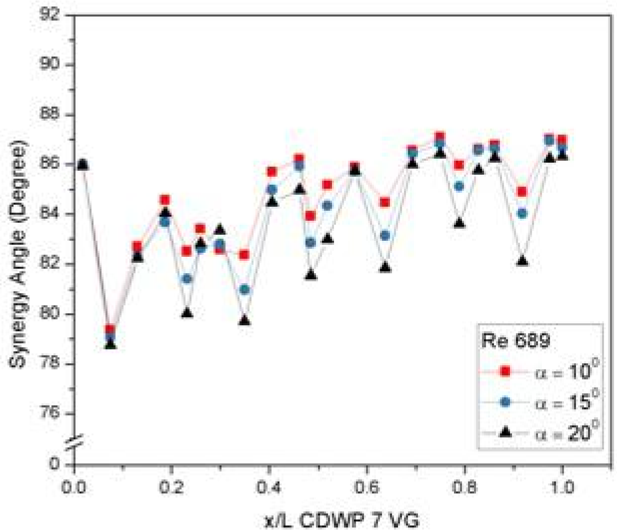

c

Figure 18. Local synergy angle under several attack angles in the case of seven pairs of VGs at Re = 689 for: a. DWP, b. CxDWP , and c. CDWP

freestream region. Whereas, δ_t is thermal boundary layer thickness.

Meanwhile, $(\bar{U}.\nabla\bar{T})$ in Equation (21) can be described as follows:

$$(\bar{U}.\nabla\bar{T}) = |\bar{U}||\nabla\bar{T}|\cos\theta \quad \text{(Eq. 22)}$$

$$\cos\theta = \frac{(\bar{U}\nabla\bar{T})}{|\bar{U}||\nabla\bar{T}|} \quad \text{(Eq. 23)}$$

where θ is the angle of intersection between the velocity vector and the temperature gradient.

Figure 18 describe the field synergy angle in the DWP, CxDWP, and CDWP cases with variations in the angles of attack for seven pairs of VGs at Re = 689. In Figure 18, it can be expressed that the generation of the high longitudinal vortex at Re = 689 reduces the intersection angle between the velocity vector and the temperature gradient [28]. Synergy angle at the installation of seven pairs of DWP, CxDWP, and CDWP are decreased to 79.74°, 79.13°, and 78.76°, respectively, with attack angles of 20° and Re = 689, as expressing in Figure 18. The decrease in synergy angle is influenced by the type of VG in which in the present study, the lowest to highest synergy angle is observed sequentially from the use of CDWP, CxDWP, and DWP. VG curvature affects the strength of the generation of longitudinal vortices in which longitudinal vortices modify the synergy between the velocity vector and the temperature gradient [25].

CONCLUSIONS:

In this study, improvements in convection heat transfer using DWP, CxDWP, and CDWP VGs by varying the angle of attack from 10º to 20º and their effect on the pressure drop were numerically analyzed in fin and tube heat exchangers. From this study, it can be concluded that the increase in the angle of attack, and the frontal area of the VG increases the intensity of the longitudinal vortex. The highest increase in vortex longitudinal intensity was obtained in the installation of CDWP of 185.23% against DWP with an angle of attack of 20º and Re = 689 at the location x/L = 0.21. This resulted in an increase in the highest convection heat transfer coefficient at seven pairs of CDWP with an attack angle of 20º and Re = 689 ie 84.85% to the baseline. However, an increase in convection heat transfer coefficient was accompanied by an increase in pressure drop of 128.74% in the installation of seven pairs of CDWP against the baseline with an angle of attack of 20° and Re = 689. Thermal-hydraulic performance was analyzed using the London goodness factor (j/f) and j/f ratio compared to variations in the angle of attack. A decrease in the j/f ratio was found to be 18.15% to the baseline for the case of seven pairs CDWP at an angle of attack of 20º and Re = 689.Then, the mechanism for improving convection heat transfer was determined by the field synergy principle. For the seven rows of CDWP with an attack angle of 20° and Re = 689, a synergy angle was obtained at 78.76° at the location x/L = 0.074.

ACKNOWLEDGMENTS:

This work was supported by the Fundamental Research of Minitry of Education and Culture, Indonesia, with contract number: 225-110/UN7.6.1/PP/2020. The authors are grateful to all research members, especially Lab. Thermofluid of Mechanical Engineering of Diponegoro University Indonesia, Department of Aerospace Engineering of Bandung State Polytechnic, Indonesia

Nomenklatur

A_T	Total area of heat transfer (m^2)	v	y-axis velocity (m/s)
A_{min}	Minimum flow area (m^2)	V_m	Average velocity at A_{min}(m/s)
B	Channel width (m)	w	z-axis velocity (m/s)
c_p	Fluid specific heat (J/(kgK))	x	Delta winglet pitch (m)
D	Tube outer diameter (m)	y	Delta winglet length (m)
D_h	Tube inner diameter (m)		
f	Friction factor	*Greek Symbols*	
F_t	Fin thickness (m)	α	Angle of attack (°)
h	Convection coefficient (W/m^{2}K)	μ	Dynamic viscosity (Pa s)
H	Channel height (m)	ρ	Density (kg/(m^3))
L	Channel length (m)	λ	Thermal conductivity (W/(mK))
N	Number of volume controls or points	β	Synergy angle (°)
Nu	Nusselt number	ϕ	Computational domain
P	Pressure (Pa)	Γ	Diffusion coefficient
P_l	Longitudinal pitch between tubes(m)	Λ	Winglet aspect ratio
P_s	Transverse pitch between tubes (m)		
ΔP	Pressure drop (Pa)	*Subscripts*	
Pr	Prandtl number	in	Inlet parameter
Q	Heat capacity (W)	m	Average value
Re	Reynolds number	out	Outlet parameter
T	Temperature (K)	w	Wall
ΔT	Average bulk temperature (K)	CDWP	Concave Delta Winglet Pairs
u	x-axis velocity (m/s)	CxDWP	Convex Delta Winglet Pairs
u_{in}	Frontal velocity (m/s)	DWP	Delta Winglet Pairs

REFERENCES:

1. Muhammad Awais, Arafat A., Heat and mass transfer for compact heat exchanger (CHXs) design: A state-of-the-art review, International Journal of Heat and Mass Transfer 127 (2018) 359–380.

2. KeWei Song, Toshio Tagawa, The optimal arrangement of vortex generators for best heat transfer enhancemen in flat-tube-fin heat exchanger, International Journal of Thermal Sciences 132 (2018) 355–367.

3. Ahmadali Gholami, Mazlan A. Wahid, H.A. Mohammed, Thermal-hydraulic performance fin-and-oval tube compact heat exchangers with innovative design of corrugated fin patterns, International Journal of Heat and Mass Transfer 106 (2017) 573–592.

4. Chi-Chuan Wang, Kuan-Yu Chen, Jane-SunnLiaw, Chih-Yung Tseng, An experimental study of the air-side performance of fin-and-tube heat exchangers having plain, louver, and semi-dimple vortex generator

configuration, International Journal of Heat and Mass Transfer 80 (2015) 281–287.

5. Huan-ling Liu, Heng Li, Ya-ling He, Zeng-tao Chen, Heat transfer and flow characteristics in a circular tube fitted with rectangular winglet vortex generators, International Journal of Heat and Mass Transfer 126 (2018) 989–1006.

6. C. Zhai, M.D. Islam, R. Simmons, I. Barsoum, Heat transfer augmentation in a circular tube with delta winglet vortex generator pairs, International Journal of Thermal Sciences 140 (2019) 480–490.

7. KeWei Song, LiangBi Wang, Effects of longitudinal vortex interaction on periodically developedflow and heat transfer of fin-and-tube heat exchanger, International Journal of Thermal Sciences 109 (2016) 206–216.

8. Assadour Khanjian, Charbel Habchi, Serge Russeil, Daniel Bougeard, Thierry Lemenand, Effect of rectangular winglet pair roll angle on the heat transfer enhancement in laminar channel flow, International Journal of Thermal Science 114 (2017) 1–14.

9. G. Lianga, M.D. Islam, N. Kharoua, R. Simmons, Numerical study of heat transfer and flow behavior in a circular tube fitted with varying arrays of winglet vortex generators, International Journal of Thermal Sciences 134 (2018) 54–65.

10. Hung-Yi Li, Wan-Rong Liao, Tian-Yang Li b, Yan-Zuo Chang, Application of vortex generators to heat transfer enhancement of a pin-fin heat sink, International Journal of Heat and Mass Transfer 112 (2017) 940–949.

11. Hemant Naik, Shaligram Tiwari, Effect of winglet location on performance of fin-tube heat exchangers with inline tube arrangement, International Journal of Heat and Mass Transfer 125 (2018) 248–261.

12. Gaofeng Lu, Xiaoqiang Zhai, Analysis on heat transfer and pressure drop of fin-and-oval-tube heat exchangers with tear-drop delta vortex generators, International Journal of Heat and Mass Transfer 127 (2018) 1054–1063.

13. Mohd. Zeeshan, Sujit Nath, Dipankar Bhanja, Numerical study to predict optimal configuration of fin and tubecompact heat exchanger with various tube shapes and spatialarrangements, Energy Conversion and Management 148 (2017) 737–752.

14. Nares Chimres, Chi-Chuan Wang, Somchai Wongwises, Optimal design of the semi-dimple vortex generator in the fin and tube heat exchanger, International Journal of Heat and Mass Transfer 120 (2018) 1173–1186.

15. Mohd Fahmi Md Salleh, Hussein A. Mohammed, Mazlan A. Wahid, Thermal and hydraulic characteristics of trapezoidal winglet across fin-and-tube heat exchanger (FTHE), Applied Thermal Engineering 149 (2019) 1379–1393.

16. Gaofeng Lu, Xiaoqiang Zhai, Effects of curved vortex generators on the air-side performance of fin-and-tubeheat exchangers, International Journal of Thermal Sciences 136 (2019) 509–518.

17. Syaiful, Experimental study of concave rectangular winglet vortex generators effect on thermal-hydrodinamic performances of airflow inside a channel, IntechOpen 2017 219–235.

18. KeWei Song, Toshio Tagawa, ZhongHao Chen, Qiang Zhang, Heat transfer characteristics of concave and convex curved vortex generators in the channel of plate heat exchanger under laminar flow, International Journal of Thermal Sciences 137 (2019) 215–228.

19. Yonggang Lei, Fang Zheng, Chongfang Song, Yongkang Lyu, Improving the thermal hydraulic performance of a circular tube by using punched delta-winglet vortex generators, International Journal of Heat and Mass Transfer 111 (2017) 299–311.

20. Zhimin Han, Zhiming Xu, Jingtao Wang, Numerical simulation on heat transfer characteristic of rectangular vortex generators with hole, Intenational Journal of Heat and Mass Transfer 126 (2018) 993–1001.

21. Mohammad Oneissi, Charbel Habchid, Serge Russeila, Thierry Lemenand, Daniel Bougeard, Heat transfer enhancement of inclined projected winglet pair vortex generators with protrusions, International Journal of Thermal Sciences 134 (2018) 541–551.

22. Syaiful, Imam Syarifudin, Maria F. Soetanto, Myung-whan Bae, Numerical simulation of heat transfer augmentation in fin-and-tube heat exchanger with various number of rows of concave rectangular winglet vortex generator, MATEC Web of Conferences 159, 02012 (2018).

23. A. Joardar, A.M. Jacobi, Heat transfer enhancement by winglet-type vortex generator arrays in compact plain-fin-and-tube heat exchanger, International Journal of Refrigeration 31 (2008) 87–97.

24. Uddin Kahyap, Koushik Das, BiplabKkumarDebnath, Effect of surface modification of a rectangular vortex generator on heat transfer rate from a surface to fluid, International Journal of Thermal Sciences 127 (2018) 61–78.

25. Amit Arora, P.M.V. Subbarao, R.S. Agarwal, Numerical optimization of location of ‘common

flow up' delta winglets for inline aligned finned tube heat exchanger, Applied Thermal Engineering 82 (2015) 329-340.

26. Ya-Xia Li, Xia Wang, Jing Zhang, Li Zhang, Jian-Hua Wua, Comparison and analysis of the arrangement of delta winglet pair vortex generators in a half coiled jacket for heat transfer enhancement, International Journal of Heat and Mass Transfer 129 (2019) 287–298.

27. Junling Xie, Yuanyuan Xie, Chris Yuan, Numerical study of heat transfer enhancement using vortex generator for thermal management of lithium ion battery 129 (2019) 1184–1193.

28. L.H. Tang, W.X. Chu, N. Ahmed, M. Zheng, A new configuration of winglet longitudinal vortex generator to enhance heat transfer in a rectangular channel, Applied Thermal Engineering 104 (2016) 74–84.

29. Vinicius Malatesta, Leandro F. Souza, Joseph T. C. Liu, Markus J. Kloker, Heat transfer analysis in a flow over concave wall with primary and secondary instabilities, Procedia IUTAM 14 (2015) 487–495.

30. Yuanbo Liu, Xuehu Ma, Xuan Ye, Yansong Chen, Yaqi Cheng, ZhongLan,Heat transfer enhancement of annular finned tube exchanger using vortexgenerators: The effect of oriented functional circumferential arrangement, Thermal Science and Engineering Progress 10 (2019) 27–35.

31. Sunil Chamoli, Ruixin Lu, Peng Yu,Thermal characteristic of a turbulent flow through a circular tube fitted with perforated vortex generator inserts, Applied Thermal Engineering 121 (2017) 1117–1134.

32. Ya-Ling He, Pan Chu, Wen-Quan Tao, Yu-Wen Zhang, Tao Xie, Analysis of heat transfer and pressure drop for fin-and-tube heat exchangers with rectangular winglet-type vortex generators, Applied Thermal Engineering 61 (2013) 770–783.

33. Z.Y. Guo, W.Q. Tao, R.K. Shah, The field synergy (coordination) principle and its applications in enhancing single phase convective heat transfer, International Journal of Heat and Mass Transfer 48 (2005) 1797–1807